Long-Range Solvent Effects on the Orbital Interaction Mechanism of Water Acidity Enhancement in Metal Ion Solutions: A Comparative Study of the Electronic Structure of Aqueous Mg and Zn Dications

Leonardo Bernasconi,*,† Evert Jan Baerends,*,† and Michiel Sprik*,†,‡

Theoretische Chemie, Vrije Universiteit Amsterdam, De Boelelaan 1083, 1081 HV Amsterdam, The Netherlands, and Department of Chemistry, University of Cambridge, Lensfield Road, Cambridge CB2 1EW, United Kingdom

Received: February 16, 2006; In Final Form: April 14, 2006

We study the dissociation of water coordinated to a divalent metal ion center, $M^{2+} = Mg^{2+}$, Zn^{2+} using density functional theory (DFT) and ab initio molecular dynamics (AIMD) simulations. First, the proton affinity of a coordinated OH^- group is computed from gas-phase $M^{2+}(H_2O)_5(OH^-)$, which yields a relative higher gas-phase acidity for a Zn^{2+}-coordinated as compared to a Mg^{2+}-coordinated water molecule, $\Delta pK_a^{gp} = 5.3$. We explain this difference on the basis of a gain in stabilization energy of the $Zn^{2+}(H_2O)_5(OH^-)$ system arising from direct orbital interaction between the coordinated OH^- and the empty 4s state of the cation. Next, we compute the acidity of coordinated water molecules in solution using free-energy thermodynamic integration with constrained AIMD. This approach yields pK_a $Mg^{2+} = 11.2$ and pK_a $Zn^{2+} = 8.4$, which compare favorably to experimental data. Finally, we examine the factors responsible for the apparent decrease in the relative Zn^{2+}-coordinated water acidity in going from the gas-phase ($\Delta pK_a^{gp} = 5.3$) to the solvated ($\Delta pK_a = 2.8$) regime. We propose two simultaneously occurring solvation-induced processes affecting the relative stability of $Zn^{2+}(H_2O)_5(OH^-)$, namely: (a) reduction of the Zn 4s character in solution states near the bottom of the conduction band; (b) hybridization between OH^- orbitals and valence-band states of the solvent. Both effects contribute to hindering the $OH^- \rightarrow Zn^{2+}$ charge transfer, either by making it energetically unfavorable or by delocalizing the ligand charge density over several water molecules.

I. Introduction

Metal ions play a central role in most catalytic and enzymatic processes. Nearly one-third of all proteins contain a metal ion, either as a cofactor or as a structure stabilizer.[1] In-depth understanding of metal binding in natural conditions is an important step in modeling enzymatic activity. This insight may also provide guidelines for developing new catalytic paths and tailoring their efficiency in artificial environments.

The aqueous chemistry of several naturally occurring metal ions is also of great importance in biochemistry, geochemistry, and catalysis. Metal ions in solution are known to enhance the acidity of coordinated water molecules. This phenomenon is typically interpreted as a manifestation of the Coulombic attraction between the positive charge localized on the metal center and the electronic charge density of the ligands.[2] Experimentally, well-defined trends in acidity for hydrated cations are observed, such as lower pK_a with increasing cation charge Z and decreasing cation radius r_M. For "hard" cations such as Li^+, Mg^{2+}, and Al^{3+}, a linear relationship exists between pK_a and Z^2/r_M. Other "soft" ions may show noticeable deviations from this behavior. Typically, acidities are enhanced for very polarizable and electronegative cations compared to hard species with a similar radius and charge. Hydrated Mg^{2+} and Zn^{2+} constitute a prototypical case study of a cation pair with contrasting hard and (moderately) soft behavior.[3] Despite the small difference in r_M (respectively, 0.65 and 0.74 Å), magnesium and zinc ions have rather different properties. Mg^{2+} often prefers oxygen ligands with an octahedral coordination arrangement, whereas Zn^{2+} can bind N, O, S, and halogen atoms with more varied coordination motifs, including tetrahedral binding sites in proteins.[3] Although experimental[4−9] and theoretical[10,11] studies have shown both ions to be hexahydrated in aqueous solution, various ab initio molecular orbital calculations[3,12−14] on gas-phase Zn^{2+}−water clusters indicate $[Zn^{2+}(H_2O)_4](H_2O)_2$ or $[Zn^{2+}(H_2O)_6]$ to be alternatively more stable, depending on the conditions chosen. No such feature has been observed in Mg^{2+}−water clusters. These findings are consistent with different biological functions: whereas Mg^{2+} has predominantly (but not exclusively; see, e.g., chlorophyll) structural roles, Zn^{2+} is typically responsible for catalytic activity in enzymes, which may involve changes in coordination number, although it may also act as a structure stabilizer as in "zinc-finger" proteins. In aqueous solution, both ions are responsible for a marked increase in acidity compared to water. The pK_a decreases from 15.7 in liquid water to 12.4 for a Mg^{2+} solution and down to ∼9.2 for hydrated Zn^{2+}.[2]

In this study, we will examine the origin of the difference in acidity between water molecules belonging to the first solvation shell of Mg^{2+} and Zn^{2+}, based on analysis of the electronic structure of the hexahydrated cation clusters in the gas-phase and in the solvated regime at finite temperature. The scope of this work is to develop a consistent molecular-orbital picture of the interaction between a water molecule (or a dissociated OH^-) and the metal center and to isolate the relative importance

* E-mail: L.Bernasconi@few.vu.nl (L.B.); baerends@few.vu.nl (E.J.B.); ms284@cus.cam.ac.uk (M.S).
† Vrije Universiteit Amsterdam.
‡ University of Cambridge.

10.1021/jp0609941 CCC: $33.50
Published on Web 05/24/2006

of solvation effects on this interaction. Combined static-DFT and AIMD simulations have been proven to provide unprecedented insight into the structure and dynamics of ionic solutions.[15−21] In this study, we will adopt a similar approach to clarify the relation between electronic structure and thermodynamic stability of species involved in dissociation reactions in solution.

Accurate pK_a values for solvated molecules can be estimated using bond-valence methods[22] and semiempirical or DFT calculations with continuum reaction-field solvation models.[23−37] The applicability of implicit solvation models to hydrated $M^{q+}(H_2O)_n$ is however questionable.[12,38,39] It has been found that the expected contraction of the M−O coordination shell upon solvation caused by charge separation in the hydrogen-bonded water ligands can only be reproduced if specific interactions between first and outer solvation shells are explicitly accounted for.[39] Long-range continuum interactions in a polarizable medium have been reported to cause the opposite effect, i.e. to increase the M−O distance.[38] For this reason, we will compute acidities using an AIMD-based approach similar to the one proposed by Davies et al.[40] and Ivanov et al.,[41,42] which is based on the statistical mechanics method described by Chandler[43] (see also ref 44; for an alternative approach based on free energy perturbation methods, see ref 45). The electronic structures of the metal ion, coordinated water molecules, and the solvent molecules are all treated explicitly within DFT. Values of pK_a are computed from free-energy profiles for deprotonation estimated by thermodynamic integration from AIMD simulations with an explicit solvent. This method is virtually parameter-free, albeit at the price of a much larger computational cost compared to implicit-solvent models. All the relevant interactions between the metal ion and the solvent and between the solvent molecules are however properly included, at least within the accuracy afforded by DFT-based AIMD and by the finite size of the simulation sample.

The paper is organized as follows. In section II, we provide various technical details regarding the calculations. In section III, calculations are described and carried out on gas-phase $Mg^{2+}(H_2O)_6$ and $Zn^{2+}(H_2O)_6$. The aim of this section is threefold: (1) to estimate the acidity of water molecules coordinated to each of the metal centers; (2) to develop an orbital model capable of explaining the difference in acidity between the two ions; (3) to identify a suitable index relating molecular orbitals with thermodynamic properties of metal-coordinated species. The latter will be used as a tool to interpret the electronic structure of the hydrated ions. In section IV, we outline the constrained AIMD thermodynamic integration procedure used to estimate pK_as, and we indicate how the orbital model describing proton abstraction in the gas phase can be generalized to the hydrolysis of coordinated water molecules in solution. Our results are briefly summarized in section V.

II. Method and Computational Details

All-electron gas-phase calculations were performed at the BLYP[46,47] level of theory using ADF[48] with a QZ4P basis set and the ZORA[49] relativistic correction. The conductor-like screening model (COSMO[50]) in the ADF implementation[51] was applied in some of the calculations described in section IV. The effective atomic radii were 1.72 and 1.30 Å for O and H, respectively.[52] For Mg^{2+} and Zn^{2+}, we used optimized BP86/TZVP values computed by Sillanpää et al.,[53] 1.45 and 1.34 Å, respectively. Condensed-phase calculations and AIMD simulations were carried out with the plane-wave pseudopotential code CPMD.[54] A periodic supercell of size $a = 9.865$ Å was adopted for both cation solutions, containing 1 metal ion and 31 water molecules. A homogeneously distributed neutralizing background was introduced to enforce charge neutrality. The Kohn−Sham eigenfunctions at the Γ point of the Brillouin zone of the supercell were expanded in plane waves up to a kinetic energy cutoff of 70 Ry.

Standard norm-conserving fully separable[55] ab initio pseudopotentials of the Troullier−Martins[56] type were used for O and H, which were extensively tested in previous calculations on various solvated systems. For Mg, we only considered the 3s orbital explicitly in the valence states, and we accounted for semicore 2p states through a nonlinear core correction.[57] The pseudopotential was obtained by inversion of an all-electron BLYP density computed for an atom in the $3s^1 3p^1$ configuration; pseudisation radii were chosen of 2.59 b for all (s, p, and d) nonlocal channels. We tested the accuracy of this pseudopotential representation by comparing to an AIMD simulation of hydrated Mg^{2+} (ref 15) carried out with explicit inclusion of Mg 2p states. Similarly, we only considered the 4s orbital as valence in the Zn pseudopotential, with a nonlinear core correction for the semicore states. This approach has been proven to yield accurate results in solid-state (covalent) systems.[58] Gaussian−Hermite integration was used, with pseudisation radii of 1.38, 1.38, and 1.90 b for s, p, and d nonlocal channels. The accuracy of the resulting pseudopotential was assessed by comparing to various static properties of gas-phase systems obtained from all-electron calculations, as well as to the solvation shell structure of hydrated Zn^{2+} evinced from extended X-ray absorption fine structure (EXAFS) experiments (section IV).[59]

Initial atomic configurations were obtained from classical molecular dynamics simulations employing an SPC/E potential for water−water interaction and standard Buckingham potentials for M^{2+}−O and M^{2+}−H interactions. Extensive AIMD equilibration (∼20 ps) was then allowed before starting production runs.

Constant-volume AIMD simulations were performed using the Car−Parrinello method[60−62] with a fictitious mass of 600 au and an integration time step of 5.1676 au. Quenching to the Born−Oppenheimer surface was carried out every ∼1 ps to guarantee good adiabaticity throughout the AIMD runs. Total simulation times were on the order of 5 ps for each step in the thermodynamic integrations (see section IV). In all simulations, H was replaced by deuterium to allow for more efficient equilibration. The temperature was set to 298 K and controlled through a Nosé−Hoover thermostat with a thermostat parameter of 400 au.

III. Gas-Phase Calculations

A. Proton Affinities. The proton affinity (PA) for a generic reaction

$$A^- + H^+ \rightarrow AH$$

is defined[2] as the negative of the reaction enthalpy[63] $-\Delta H = -\Delta E + RT$, where $R = 8.314$ J K mol^{-1} and $T = 298.15$ K. We consider the following reactions in the gas phase:

$$OH^- + H^+ \rightarrow H_2O \quad (1)$$

$$Mg^{2+}(H_2O)_5(OH^-) + H^+ \rightarrow Mg^{2+}(H_2O)_6 \quad (2)$$

and

$$Zn^{2+}(H_2O)_5(OH^-) + H^+ \rightarrow Zn^{2+}(H_2O)_6 \quad (3)$$

TABLE 1: Geometric Parameters for Optimized Gas-Phase Structures[a]

	d[M−O_{H_2O}]	d[M−O*]	a[M−Ô*−H]
$Mg^{2+}(H_2O)_6$	2.119	2.119	127.17
$Mg^{2+}(H_2O)_5(OH^-)$	2.150 2.149 2.124 2.123 2.190	1.940	144.87
$Zn^{2+}(H_2O)_6$	2.142	2.142	126.36
$Zn^{2+}(H_2O)_5(OH^-)$	2.273 2.396 2.059 2.197 2.566	1.862	116.86

[a] Distances are in angstroms, and angles are in degrees. O* indicates the oxygen atom of the water molecule whose proton is abstracted in going from $M^{2+}(H_2O)_6$ to $M^{2+}(H_2O)_5(OH^-)$.

The structures of the protonated $Mg^{2+}(H_2O)_6$ and $Zn^{2+}(H_2O)_6$ and deprotonated $Mg^{2+}(H_2O)_5(OH^-)$ and $Zn^{2+}(H_2O)_5(OH^-)$ complexes were optimized by allowing small initial random displacements (∼0.01 Å) from an ideal (pseudo-)octahedral geometry (vide infra) and, then, performing an optimization with no symmetry constraints imposed. Convergence criteria were 5×10^{-4} au and 5×10^{-3} au in the total energy and gradients, respectively. Selected structural parameters for these complexes are shown in Table 1. From eq 1, we computed a PA for a free OH^- group $-\Delta H = 1629$ kJ mol^{-1}, which compares satisfactorily to the experimental value, $-\Delta H = 1635$ kJ mol^{-1}.[2] From eqs 2 and 3, we obtained PAs of 694 and 663 kJ mol^{-1} for a Mg^{2+}-coordinated and Zn^{2+}-coordinated hydroxide ion, respectively.

A large decrease in the PA of coordinated OH^- relative to its gas-phase counterpart (∼940 kJ mol^{-1}) contrasts here with a comparatively modest difference between water molecules coordinated to the two different ion centers (31 kJ mol^{-1}). The difference between coordinated and free OH^- is explained by the stabilization arising from coordination to a cation with a large positive charge. As will be shown in due course, the additional stabilization of a Zn^{2+}-coordinated OH^- arises both from Coulombic effects (caused by a shorter metal−OH^- distance and by the orientation of the OH^- group) and from specific Zn^{2+}−OH^- orbital interactions.

For the sake of comparison to calculations on the solvated systems (section IV), we define a relative gas-phase acidity as $\Delta pK_a^{gp} = -\log(K^{gp}_{Zn^{2+}}/K^{gp}_{Mg^{2+}})$. $K^{gp}_{Zn^{2+}}/K^{gp}_{Mg^{2+}}$ is the equilibrium constant for the proton-transfer reaction

$$Mg^{2+}(H_2O)_6 + Zn^{2+}(H_2O)_5(OH^-) \rightarrow Zn^{2+}(H_2O)_6 + Mg^{2+}(H_2O)_5(OH^-)$$

given by

$$\frac{K^{gp}_{Zn^{2+}}}{K^{gp}_{Mg^{2+}}} = e^{-\Delta\Delta G/RT} \quad (4)$$

with

$$\Delta\Delta G = \Delta G(Mg^{2+}) - \Delta G(Zn^{2+}) \quad (5)$$

$\Delta G(Mg^{2+})$ and $\Delta G(Zn^{2+})$ are free energy differences computed by rearranging eqs 2 and 3, and they yield $K^{gp}_{Zn^{2+}}/K^{gp}_{Mg^{2+}} = 5.5 \times 10^{-6}$ or $\Delta pK_a^{gp} = 5.3$. The latter value indicates that the acidity of a Zn^{2+}-coordinated water molecule in the gas phase is substantially higher than that of a Mg^{2+}-coordinated one. This estimate largely exceeds the experimental difference in pK_a for the solvated ions, $pK_a(Mg^{2+}) - pK_a(Zn^{2+}) \simeq 3$.[2] The origin of this difference will be examined in detail in section IV.

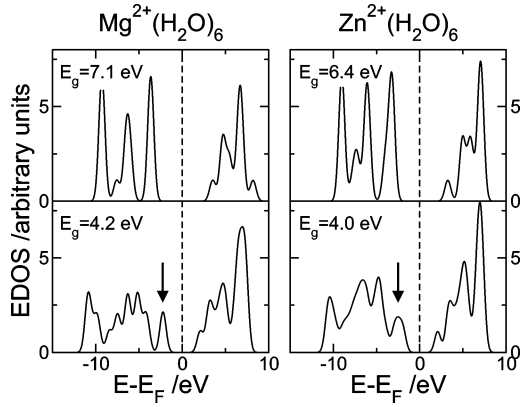

Figure 1. Kohn−Sham EDOS of optimized gas-phase hydrated M = Mg, Zn cation complexes. The upper panels are for $M^{2+}(H_2O)_6$, and the lower panels, for $M^{2+}(H_2O)_5(OH^-)$ systems. All plots have been aligned at $E_F = (E_{LUMO} - E_{HOMO})/2$ for comparison. E_g is the band gap. Arrows indicate the *intra*gap states (see main text for details). A Gaussian smearing of a standard deviation of 0.25 eV has been added to all EDOS plots.

B. Origin of the Enhanced Acidity in Zn^{2+}-Coordinated Water. In eqs 1−3, all reagents are assumed to be at infinite separation. This fact entails that chemical equilibria will in all cases be determined solely by the thermodynamic stability of OH^- (or of the ionic species containing OH^-) relative to the undissociated species in the right-hand side (rhs) of each equation. Factors stabilizing $Zn^{2+}(H_2O)_5(OH^-)$ in preference to $Mg^{2+}(H_2O)_5(OH^-)$ will therefore increase the relative acidity of a water molecule coordinated to Zn^{2+}.

In Figure 1, we compare the (valence) Kohn−Sham energy density of states (EDOS) for undissociated $M^{2+}(H_2O)_6$ and dissociated $M^{2+}(H_2O)_5(OH^-)$ systems. All plots refer to fully optimized structures. In both cases, lowering of the octahedral symmetry results in the disappearance of several degeneracies within the occupied manifold of states and a more dispersed overall EDOS profile. The energy gap E_g decreases by 2.9 and 2.4 eV in the Mg^{2+} and Zn^{2+} systems, respectively. Virtual states are comparatively unaffected.

The reduction of the energy gap occurs as a consequence of the promotion of a composite of states (indicated by arrows in the lower plots of Figure 1) to within the forbidden-gap region of the octahedral complexes. In both cases, the two molecular orbitals of higher energy (corresponding to the complex HOMO and HOMO-1) correspond to almost pure OH^- 1π orbitals (Figure 2; see also Table 2). The lobes of the higher energy orbital are above and below the M^{2+}−O−H plane. This state will conventionally be labeled $1\pi_y$. The second lowest-energy orbital ($1\pi_x$) extends approximately in the M^{2+}−O−H plane. The smaller M^{2+}ÔH angle in the Zn^{2+} complex allows the $1\pi_x$ orbital (which extends perpendicularly to $1\pi_y$ and to a lower energy O−H σ orbital) to point almost exactly toward the metal center, and one of its lobes therefore occupies the M^{2+}−O region. The larger angle in $Mg^{2+}(H_2O)_5(OH^-)$ prevents this favorable geometric orbital arrangement from occurring. (Table 1).

The third (HOMO-2) *intra*gap state in $Zn^{2+}(H_2O)_5(OH^-)$ is an almost pure $1b_1$ (or $1b_2$) "π-lonepair" localized on one water molecule. In the optimized complex structure, this molecule resides at a larger distance from the metal center than the remaining four coordinated molecules. Lower-energy states (not belonging to *intra*gap manifolds) retain $1b_1$-$1b_2$ character, similar to the undissociated $M^{2+}(H_2O)_6$ systems. It may therefore be argued that the separation of this state from low energy $1b_1$-$1b_2$ combinations reflects an overall destabilization of orbitals

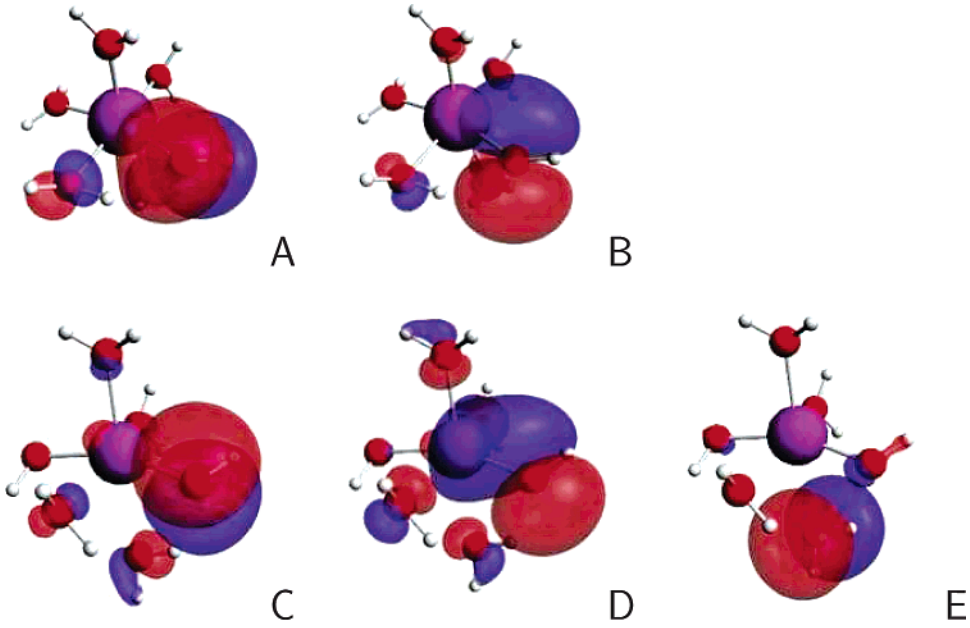

Figure 2. *Intra*gap states of gas-phase optimized $Mg^{2+}(H_2O)_5(OH^-)$ (A and B) and $Zn^{2+}(H_2O)_5(OH^-)$ (C−E). A and C correspond to the HOMO, B and D, to the HOMO-1 of each complex. E is the HOMO-2 of $Zn^{2+}(H_2O)_5(OH^-)$. Isosurfaces are plotted corresponding to 0.03 electrons/Å^3, and different colors indicate the phase of the orbitals. The metal atom is at the center of each plot, and all orbitals have a node on the O atom of the OH^- group.

TABLE 2: Selected Kohn−Sham Orbital Energies and Contributions from Fragment Orbitals (Percentages) for Gas-Phase $M^{2+}(H_2O)_6$ and Corresponding Dissociated Species in the Pseudo-octahedral ([po]; See Main Text) and Optimized Geometries[a]

	HOMO		HOMO-1		HOMO-2	
$Mg^{2+}(H_2O)_6$	−16.208	51.08 H_2O $1b_2$ 16.62 H_2O $1b_1$ 12.01 H_2O $1b_2$ 11.29 H_2O $1b_2$ 4.84 H_2O $1b_1$	−16.215	44.80 H_2O $1b_1$ 30.05 H_2O $1b_1$ 13.40 H_2O $1b_2$ 4.63 H_2O $1b_2$	−16.224	58.06 H_2O $1b_2$ 12.28 H_2O $1b_2$ 10.50 H_2O $1b_1$ 7.04 H_2O $1b_1$ 6.57 H_2O $1b_2$
$Mg^{2+}(H_2O)_5(OH^-)$ [po]	−7.120	94.49 OH^- $1\pi_y$	−7.300	89.88 OH^- $1\pi_x$	−10.967	87.65 OH^- 3σ
$Mg^{2+}(H_2O)_5(OH^-)$	A −9.416	62.28 OH^- $1\pi_y$ 26.28 OH^- $1\pi_x$	B −9.586	65.37 OH^- $1\pi_x$ 26.21 OH^- $1\pi_y$	−11.317	73.20 H_2O $1b_2$ 15.80 H_2O $1b_2$
$Zn^{2+}(H_2O)_6$	−16.066	49.23 H_2O $1b_2$ 47.77 H_2O $1b_1$	−16.070	51.85 H_2O $1b_1$ 44.96 H_2O $1b_1$	−16.076	51.00 H_2O $1b_2$ 45.29 H_2O $1b_2$
$Zn^{2+}(H_2O)_5(OH^-)$ [po]	−7.499	94.85 OH^- $1\pi_y$	−7.845	83.58 OH^- $1\pi_x$ 4.74 Zn 4s	−11.099	71.55 OH^- 3σ 8.96 Zn $3d_{x^2-y^2}$ 6.50 H_2O $1b_1$
$Zn^{2+}(H_2O)_5(OH^-)$	C −9.973	65.57 OH^- $1\pi_y$ 22.31 OH^- $1\pi_x$	D −10.303	47.51 OH^- $1\pi_x$ 16.64 OH^- $1\pi_x$ 7.57 H_2O $1b_1$ 5.69 Zn $3d_{x^2-y^2}$ 4.09 H_2O $1b_1$ 3.92 Zn 4s	E −10.675	87.49 H_2O $1b_2$ 5.69 OH^- $1\pi_x$

[a] Labels for the states of $Mg^{2+}(H_2O)_5(OH^-)$ and $Zn^{2+}(H_2O)_5(OH^-)$ are as in Figure 2.

belonging to the far-water fragment, caused by decrease in the Coulombic interaction with the metal center. The absence of such a water state in the gap region of $Mg^{2+}(H_2O)_5(OH^-)$ is a consequence of the relative higher stability of the coordination shell to dissociation of one water molecule in this system and to its less distorted structure.

Differences in the equilibrium structures of $Mg^{2+}(H_2O)_5(OH^-)$ and $Zn^{2+}(H_2O)_5(OH^-)$ complicate considerably the analysis of factors responsible for the larger $1\pi_y/1\pi_x$ separation in the latter. For this reason, we considered two alternative gas-phase structures, obtained from optimized $Mg^{2+}(H_2O)_6$ and $Zn^{2+}(H_2O)_6$ by abstraction of H^+ from one water molecule, without re-optimization. We refer to these systems as "pseudo-octahedral" Mg^{2+} and Zn^{2+} complexes. They have analogous symmetry, and the $M^{2+}-O$ distances are 2.119 and 2.142 Å, respectively. We would then expect Coulomb interactions between OH^- orbitals and M^{2+} to be similar in the two cases. We computed $1\pi_y/1\pi_x$ splittings $\Delta = E_{1\pi_y} - E_{1\pi_x} = 0.163$ and 0.346 eV in $Mg^{2+}(H_2O)_5(OH^-)$ and $Zn^{2+}(H_2O)_5(OH^-)$, respectively. Despite the large decrease in Δ for the latter complex as compared to the fully optimized structure ($\Delta = 0.543$ eV), the splitting remains more pronounced in the Zn^{2+} complex, notwithstanding the slightly larger distance of OH^- from the metal center relative to the Mg^{2+} system. This fact indicates that a purely electrostatic (charge−charge) model for the $Zn^{2+}-OH^-$ interaction may be incomplete. We will now propose an interpretation of this deviation from the Coulombic limit based on mixing between orbitals of the (perturbed) Zn^{2+} and OH^- moieties. We will describe in section IV how this orbital model needs to be modified when carried over to the condensed-phase regime.

We start by considering the two fragments $Zn^{2+}(H_2O)_5$ and OH^- at infinite separation (Figure 3). Again, geometries are kept fixed as in the corresponding pseudo-octahedral system.

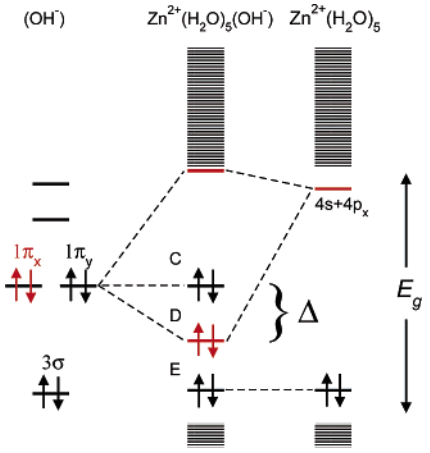

Figure 3. Schematic representation of the origin of *intra*gap states (C, D, and E) in $Zn^{2+}(H_2O)_5(OH^-)$. Energy levels of the OH^- and $Zn^{2+}(H_2O)_5$ fragments are shown on the left and right, respectively (absolute orbital energies have been rescaled for convenience). Labeling of states in $Zn^{2+}(H_2O)_5(OH^-)$ is as in Figure 2. E_g conventionally indicates the difference in energy between the HOMO-3 and LUMO of $Zn^{2+}(H_2O)_5(OH^-)$ (see main text for explanation). Dashed lines indicate the orbital interactions responsible for selective stabilization of the OH^- $1\pi_x$ relative to the OH^- $1\pi_y$ state. Δ is the separation between the two states in the complex $Zn^{2+}(H_2O)_5(OH^-)$.

In this limit, the doubly occupied $1\pi_y$ and $1\pi_x$ frontier orbitals of OH^- are degenerate, and they lie ~3.7 eV (within the BLYP approximation to DFT) above the 3σ state. The lowest unoccupied orbital of $Zn^{2+}(H_2O)_5$ has a large (53.18%) Zn 4s character. Admixture of some Zn 4p character (6.50%) results in an asymmetric distribution, with a larger contribution in the region of the "missing" OH^- ligand. When the two fragments are brought to equilibrium distance, the (electrostatically stabilized) OH^- 1π states are sufficiently close in energy to the $Zn^{2+}(H_2O)_5$ LUMO to establish proper orbital interaction. Owing to orbital symmetry, overlap with this state will only be nonvanishing in the $1\pi_x$ state case. This interaction will lower the energy of the resulting charge-transfer state (carrying 4.74% Zn 4s character) relative to the $1\pi_y$ orbital, therefore contributing to increase the absolute value of the splitting parameter Δ.

The analysis can be carried over, qualitatively unchanged, to the fully optimized $Zn^{2+}(H_2O)_5(OH^-)$. The rearrangement of the complex structure upon geometry optimization brings the OH^- group closer to the metal center, with suitable orientation to favor the $1\pi_x \rightarrow$ Zn 4s charge transfer (Table 1). Particularly noticeable is the large decrease in the Zn−Ô*−H angle (where O* is the oxygen atom of the OH^- group), from 126.36° in the pseudo-octahedral to 116.86° in the optimized structure, with the $1\pi_x$ orbital of OH^- pointing almost exactly toward the metal ion. Such behavior is not observed in the magnesium complex: the Mg−Ô*−H *increases* during geometry optimization from 127.17° to 144.87°, most likely a consequence of the larger steric repulsion with the coordinated water molecules. The strength of the (predominantly Coulombic) OH^-−Mg^{2+} is in this case not sufficient to destabilize the cation coordination shell. Referring back to eqs 2 and 3, we can show that the larger M^{2+}−OH^- orbital interaction in $Zn^{2+}(H_2O)_5$ relative to $Mg^{2+}(H_2O)_5$ accounts *quantitatively* for the difference in PA between the two species. To this aim, we decompose[64] the total interaction energy differences ΔE between fragments in $M^{2+}(H_2O)_5(OH^-)$ and $M^{2+}(H_2O)_6$ into an orbital interaction energy

$$\Delta\Delta E_{oi} = \Delta E_{oi}[Zn^{2+}(H_2O)_5(OH^-)] - \Delta E_{oi}[Zn^{2+}(H_2O)_6] - \Delta E_{oi}[Mg^{2+}(H_2O)_5(OH^-)] - (\Delta E_{oi}[Mg^{2+}(H_2O)_6]) \quad (6)$$

and a steric interaction energy, including electrostatic and Pauli repulsion effects,

$$\Delta\Delta E_{steric} = \Delta E_{steric}[Zn^{2+}(H_2O)_5(OH^-)] - \Delta E_{steric}[Zn^{2+}(H_2O)_6] - (\Delta E_{steric}[Mg^{2+}(H_2O)_5(OH^-)] - \Delta E_{steric}[Mg^{2+}(H_2O)_6]) \quad (7)$$

In addition, we define a reorganization energy difference $\Delta\Delta E_r$ corresponding to the change in total interaction energy for the $M^{2+}(H_2O)_5$ fragment in going from its pseudo-octahedral (i.e., as part of the undissociated complex $M^{2+}(H_2O)_6$) to its fully relaxed structure (as in the optimized dissociated complex $M^{2+}(H_2O)_5(OH^-)$). This decomposition yields

$$\Delta\Delta E_{oi} = 661 - 691 = -71 \text{ kJ mol}^{-1}$$

$$\Delta\Delta E_{steric} = -250 - (-180) = 39 \text{ kJ mol}^{-1}$$

$$\Delta\Delta E_r = 135 - 134 = -1 \text{ kJ mol}^{-1}$$

$$\Delta\Delta E = \Delta E_{oi} + \Delta E_{steric} + \Delta E_r = -31 \text{ kJ mol}^{-1} \quad (8)$$

The large gain in orbital interaction is counterbalanced by the unfavorable steric contribution, which is likely to arise from the Pauli repulsion between OH^- and occupied metal-ion states. This effect is more pronounced in the $Zn^{2+}(H_2O)_5(OH^-)$ complex owing to the shorter OH^-−M^{2+} distance. The reorganization energy contribution is virtually vanishing, despite the large magnitude of the individual Zn^{2+} and Mg^{2+} terms in the third equation of eqs 8.

In summary, we have studied in this section the dissociation of a water molecule in the coordination shell of gas-phase $Mg^{2+}(H_2O)_6$ and $Zn^{2+}(H_2O)_6$. A Zn^{2+}-coordinated water molecule was found to be ~5 logarithmic units more acidic than a Mg^{2+}-coordinated one. We showed that this difference arises from selective stabilization of the dissociated $Zn^{2+}(H_2O)_5(OH^-)$ complex caused primarily by OH^-−Zn^{2+} orbital interaction (OH^- $1\pi_x \rightarrow$ Zn 4s charge transfer). We proposed an orbital energy splitting parameter Δ as a direct measure of the magnitude of the orbital interaction, defined as the difference in energy between the $1\pi_y$ orbital of OH^- and the 4s-hybridized $1\pi_x$. We expect Δ to reflect variations in the coordinated-water dissociation constant, larger Δ indicating stronger relative acidity.

IV. Aqueous Mg^{2+} and Zn^{2+}

A. Calculation of pK_as. We show in Figure 4 M−O pair distribution functions ($g(r)$) and running coordination numbers $n(r)$ for the two cation solutions. A well-defined first solvation shell is observed in both cases, $n(r)$ integrating to six oxygens at 2.731 and 2.643 Å in Mg^{2+} and Zn^{2+}, respectively. The maximum of the first peak in hydrated Mg^{2+} occurs at 2.104 Å, in agreement with the X-ray diffraction estimate, 2.09 ± 0.04 Å,[65] and with results from AIMD simulations[15] carried out at the PBE level of theory, 2.13 Å. For Zn^{2+}, we find a first peak at 2.065 Å, consistent with X-ray absorption measurements,[59] 2.06 ± 0.02 Å, and with classical molecular dynamics simulations,[66] 2.08 Å. We notice that, for both cations, solvation brings about a contraction of the first solvation shell compared to gas-phase $Mg^{2+}(H_2O)_6$ and $Zn^{2+}(H_2O)_6$ (Table 1), consistent with the observations of ref 12.

We computed pK_as from free-energy profiles for deprotonation in solution. At variance with ref 40, we use as the explicit order parameter q, the distance between O and one H atom of

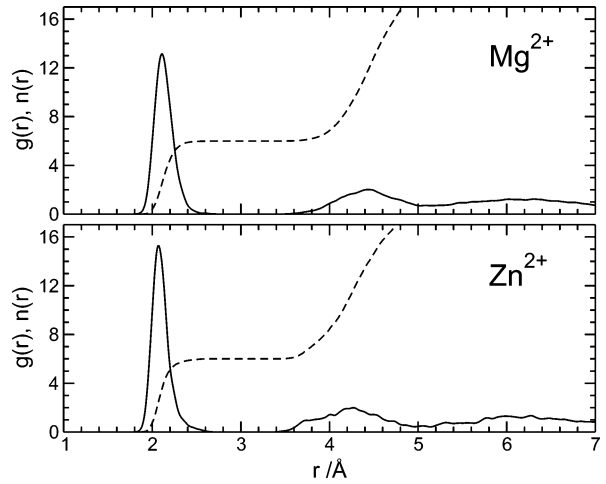

Figure 4. M−O pair distribution functions $g(r)$ (continuous line) and running coordination number $n(r)$ for hydrated Mg^{2+} and Zn^{2+} at 298 K.

a water molecule belonging to the first solvation shell of the cation r_{OH}. A series of AIMD runs is performed in each of which q is mechanically constrained to a fixed value. For each run, the mean force $f(q)$ is evaluated from the unbiased time average of the Lagrange parameter $\langle\lambda\rangle_q$ obtained by solving the equations of motion of the system with the imposed constraint:[67,68]

$$f(q) = \langle\lambda\rangle_q - \frac{2k_BT}{q} \tag{9}$$

with $k_B = 1.38 \times 10^{-23}$ J K^{-1}. The potential of mean force $w(q)$ is then estimated numerically relative to its value in some reference state q_0:

$$w(q) = w(q) - w(q_0) = -\int_{q_0}^{q} f(q')\,dq' \tag{10}$$

where $q \equiv r_{OH}$. A similar approach was used by Trout and Parrinello[69] in the computation of the free energy for O−H bond breaking in solution. The O−H radial distribution function and the potential of mean force are related by[43,40]

$$g(r_{OH}) = \exp[-w(r_{OH})/k_BT] \tag{11}$$

The dissociation constant for the reaction $H_2O \rightarrow H^+ + OH^-$ is given by

$$K(R_c) = [C_0 \int_0^{R_c} dr_{OH}\, 4\pi r_{OH}^2 \exp[-w(r_{OH})/k_BT]]^{-1} \tag{12}$$

as a function of the integration parameter R_c. This can be interpreted as the minimum O−H distance at which the bond is to be considered broken. An approximate procedure for determining the value of R_c at which the actual dissociation constant should be computed will be detailed below. C_0 is the standard concentration equal to 1 M.

The O−H radial distribution function is normalized to unity,

$$\frac{1}{V}\int_V \exp[-w(r_{OH})/k_BT]\,d\mathbf{r} = 1 \tag{13}$$

where $V = a^3$ is the supercell volume. This allows the partial reduction of the systematic error associated with the finite size of the periodic simulation supercell in the estimate of the reference $w(r_{OH})$. Rigorously, eq 12 holds under the assumption that $w(r_{OH})$ is the total work needed to bring the reactants, M^{2+}-coordinated OH^- and H^+, from infinite separation to bond distance. Owing to the use of periodic boundary conditions, only finite separations are possible, up to $r_{OH} = a/2$. The normalization condition enforces the infinite-dilution limit for a weak dissociating acid by imposing an arbitrary reference energy for the potential of mean force (see below for further details).

The second (and most important) source of error is the spurious interaction between charges in neighboring simulation cells, which prevents reliable estimates of *absolute* potentials of mean force from being obtained with this method. This interaction does however contribute by the same amount for systems of like charge, which allows *relative* acidities to be estimated. It may however remain problematic in comparisons between systems with different charge. For this reason, we anticipate a large error (on the order of 1 or more pK units) in the calculated acidity of a Mg^{2+}- or Zn^{2+}-coordinated water molecule relative to clean water, but we expect the experimental acidity of water coordinated to one cation species relative to the other to be reproducible at substantially higher accuracy.[40]

The acid dissociation constant dependence on R_c is now given by

$$K_a(R_c) = \frac{\alpha(R_c)^2}{1 - \alpha(R_c)}\frac{N}{C_0V} \tag{14}$$

where $N = 1$ is the number of reactive sites. The dissociation fraction

$$\alpha(R_c) = 1 - \frac{\int_0^{R_c} 4\pi r_{OH}^2 \exp[-w(r_{OH})/k_BT]\,dr_{OH}}{\int_0^{V^{(1/3)/2}} 4\pi r_{OH}^2 \exp[-w(r_{OH})/k_BT]\,dr_{OH}} \tag{15}$$

represents the fraction of the dissociated proton which is present within a sphere of radius R_c centered on the reactive O atom. A similar procedure can also be applied to the estimate of the dissociation constant of clean liquid water,

$$K_w(R_c) = \left[\frac{\alpha(R_c)N}{C_0V}\right] \tag{16}$$

where N is now set to the total number of water molecules in the supercell. The latter formula will be used for reference in the pK_a calculations below.

We compare in Figure 5 (upper panel) the relative mean force f profile for dissociation as a function of the order parameter r_{OH} for water coordinated to Mg^{2+} and Zn^{2+}. AIMD simulations of overall duration ∼5 ps were performed for r_{OH} ranging from 1.0 to 1.6 Å. The value of the mean force at $r_{OH} = 1.6$ Å was set as reference ($f = 0$) for both curves. The initial ($r_{OH} \simeq 1.0-1.2$) decrease in the mean force occurs in consequence to a restoring mechanism opposing the O−H bond stretching imposed by the constraint. The minimum reflects a transition from covalent interactions to a weaker electrostatic attraction between the fragments, perturbed by progressive creation of a bond between the abstracted H^+ and one of the surrounding water molecules. The final tendency toward plateauing represents the formation of an ion pair $[(H_2O)_5-M^{2+}(OH^-)-(H_3O^+)]_{aq}$ with the proton transferred to a solvent water molecule which is being prevented from diffusing freely by the presence of the constraint.[70] The corresponding potentials of mean force obtained from eq 10 are shown in the lower panel of Figure 5. As expected, an overall decrease in free energy is observed in going from clean water to a M^{2+}-coordinated water molecule (pK_a = 11−9).

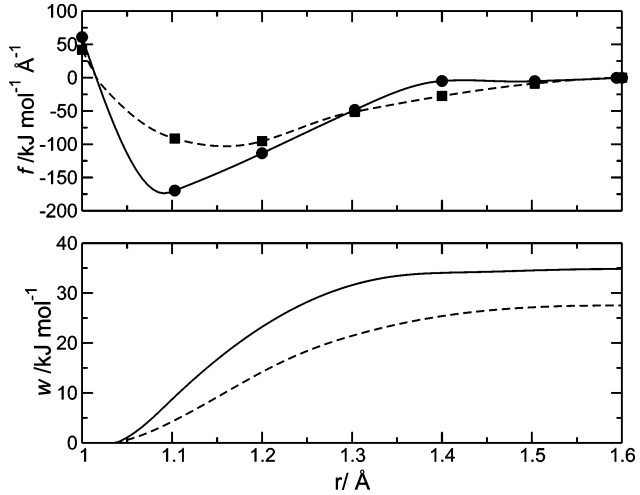

Figure 5. (upper panel) Mean force of constraint for deprotonation of Mg^{2+}-coordinated (circles) and Zn^{2+}-coordinated (squares) water molecules. The lines are spline curves interpolating the calculated values. (lower panel) Free-energy profile for Mg^{2+} (continuous line) and Zn^{2+} (dashed line) obtained from eq 10.

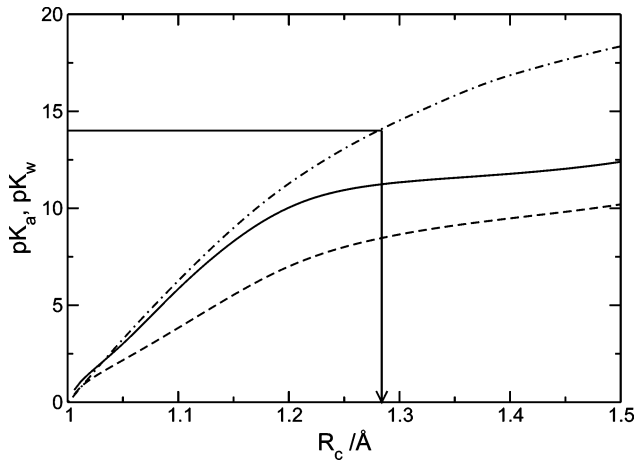

Figure 6. Estimate of pK_as. The dotted−dashed curve represents the dependence of the ionic product of water obtained from eq 16 on the integration threshold R_c. Free-energy values are from ref 69. The continuous and dashed curves are pK_a dependences on R_c for Mg^{2+}- and Zn^{2+}-coordinated water molecules, respectively, from eq 14. The vertical line represents the value of R_c at which $-\log K_w$ equals 14. The intercept of this line with each of the lower curves yields the absolute pK_a values used in this work.

The pK_a curves obtained from eq 14 are shown in Figure 6, together with the dependence of the ionic product of water pK_w $= -\log K_w$ on R_c, computed from eq 16 using free-energy values from ref 69. The latter curve is used to estimate the integration radius R_c at which the value of the pK_a for cation-coordinated water molecules should be computed.[40] On the basis of the assumption that a similar criterion for bond breaking should be used for clean and cation-coordinated water, we compute the value of R_c, yielding the ionic product of water, p$K_w(R_c) = 14$. This gives $R_c = 1.28$ Å, a value which is, as expected, well beyond the minimum of the free-energy curves for the cation-coordinated water molecules (Figure 5). The pK_as of coordinated water can now be estimated, and we obtain p$K_a(R_c = 1.28$ Å$) = 11.2$ and 8.4 for Mg^{2+} and Zn^{2+}, respectively. The increase in acidity in going from clean to Mg^{2+}-coordinated water is overestimated by ∼1 pK_a unit. The experimental difference in pK_a between Mg^{2+}- and Zn^{2+}-coordinated water (∼3 units) is however successfully reproduced. A substantial decrease in the difference of acidity between Zn^{2+}- and Mg^{2+}-coordinated water molecules compared to gas-phase $M^{2+}(H_2O)_6$ complexes is observed, from 5.3 (section III) to 2.8 pK units. In the next section, we will examine possible factors responsible for this acidity-damping effect occurring on solvation.

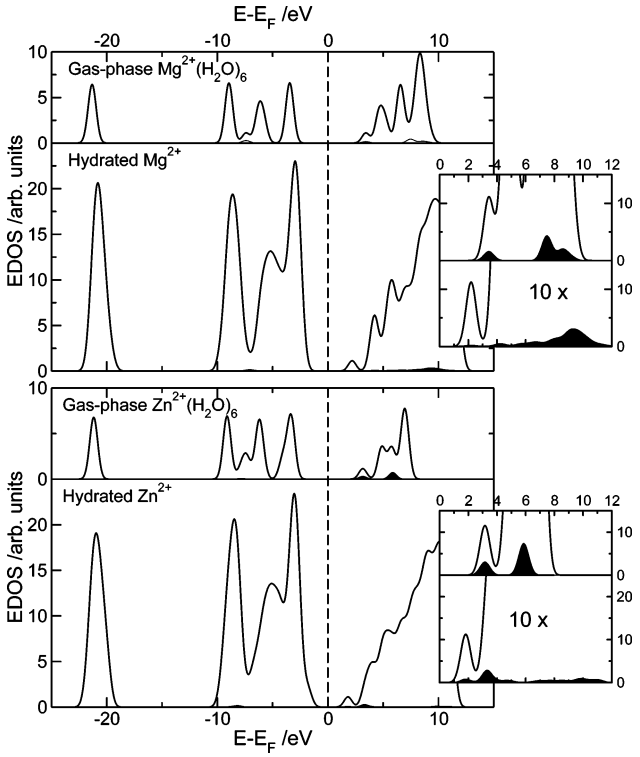

Figure 7. EDOS of gas-phase $Mg^{2+}(H_2O)_6$ and hydrated Mg^{2+} (upper panels) and of $Zn^{2+}(H_2O)_6$ and hydrated Zn^{2+} (lower panels). The black areas represent the partial density of states for the Mg 3s and Zn 4s orbitals. The insets show enlargements of the lowest portion of the virtual manifold of states for the gas-phase systems and for the conduction band for the solutions. All plots have been aligned at $E_F = (E_{LUMO} - E_{HOMO})/2$.

B. $1\pi_y/1\pi_x$ Orbital Splitting in Solution. Both hydrated undissociated $M^{2+}(H_2O)_6$ and dissociated $M^{2+}(H_2O)_5(OH^-)$ retain a well-defined stable first coordination shell on the time scale of the simulations. Some of the results of the electronic structure analysis carried out on the isolated systems will thus be used as guidelines for interpreting the dissociation behavior of coordinated water molecules in solution. Although an energy decomposition into individual bond components is not directly achievable for an infinite periodic system, properties of one-particle orbitals in the isolated complexes may be retained partially during solvation. We will show that the orbital splitting parameter Δ introduced in section III as a measure of the degree of covalency in the $M^{2+}-OH^-$ bond can also be estimated in solution and that it may be regarded as carrying an analogous significance as that for the gas-phase species. In the following, we will consider the ion-pair limit $r_{OH} = 1.6$ Å, in which a proton from a coordinated water molecule is effectively transferred to a solvent molecule, as the "fully dissociated" regime.

EDOS plots for the two solutions are shown in Figure 7, and compared to the corresponding EDOS for optimized gas-phase $M^{2+}(H_2O)_6$. For clarity, we consider here one AIMD instantaneous configuration only. We also show the partial EDOS of the 3s (Mg^{2+}) and 4s (Zn^{2+}) states as shaded areas. In both solutions, states near the top of the valence band have π-lonepair character and they may be localized on one or a few more water molecules. The nature of orbitals at the bottom of the conduction band differs in aqueous Mg^{2+} and Zn^{2+}. In the latter, LUMO and LUMO+1 carry a noticeable contribution from the Zn 4s

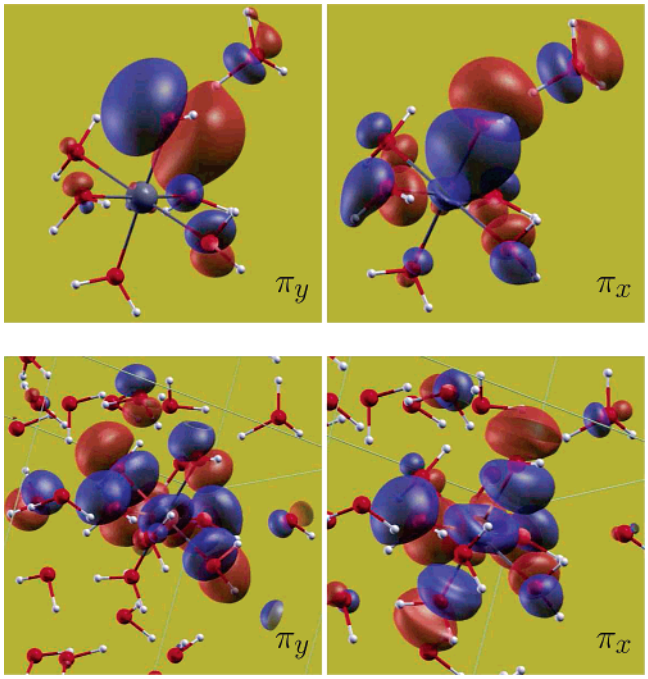

Figure 8. Figures of the π_y and π_x orbitals of one instantaneous AIMD configuration of $Zn^{2+}(H_2O)_5(OH^-)(H_3O^+)$. The two upper panels refer to the isolated system, in which all solvent water molecules have been removed by keeping the positions of the remaining atoms fixed. The lower panels are orbitals for the corresponding hydrated system. The metal ion is near the center of each plot, and H_3O^+ is in the upper right corner.

atomic orbital, yet acquiring extended-state features from hybridization with the $4a_1$ band of the solvent. By contrast, a negligible contribution from cation orbitals is observed in the lowest empty states of hydrated Mg^{2+}. This is consistent with the electronic structure of the $M^{2+}(H_2O)_6$ systems in the gas phase.

After dissociation, orbitals similar to those of the gas-phase $1\pi_y/1\pi_x$ pair appear in the upper region of the valence band of both cation solutions. They differ from the corresponding gas-phase counterparts because of their high degree of hybridization with solvent states. This is particularly evident in the case of Zn^{2+} (Figure 8). The effect is much more noticeable for the lower-energy π_x-like state which is typically located well inside the valence band, whereas the π_y-like state may occasionally appear as a true *intra*gap state slightly above the valence band edge, depending on the AIMD configuration considered.

As a consequence of this orbital mixing the $1\pi_y/1\pi_x$ pair is replaced by two manifolds of states inside, or near the edge of, the valence band. This fact renders a direct estimate of the parameter Δ by inspection of the energies of the single particle wave functions unfeasible. To locate with sufficient accuracy the center of the $1\pi_y$ and $1\pi_x$ manifolds, we used a projection of the Kohn−Sham eigenfunctions onto pseudo-atomic wave functions obtained by solving the radial Kohn−Sham equation with pseudopotentials replacing the full all-electron potentials. Maxima in the pseudo-$2p_y$ and pseudo-$2p_x$ orbitals of the O atom belonging to the dissociated OH^- group were used to assign well-defined energy values to the $1\pi_y$ and $1\pi_x$ bands and to estimate the value of Δ. This analysis was repeated for both cations over 30 AIMD configurations equally spaced in time and spanning an overall simulation time of 3 ps (Figure 9). The thermally averaged values thus obtained were $\langle\Delta\rangle = 0.249$ eV (with $\sigma = (\langle\Delta^2\rangle - \langle\Delta\rangle^2)^{1/2} = 0.089$ eV) for Mg^{2+} and $\langle\Delta\rangle = 0.483$ eV (with $\sigma = 0.109$ eV) for Zn^{2+}.

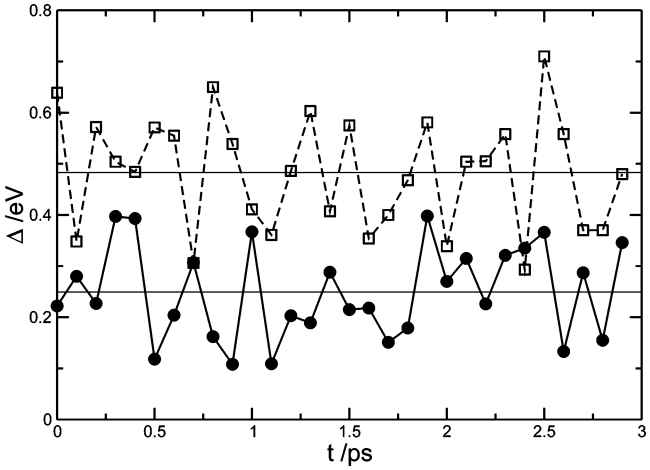

Figure 9. Time evolution of the orbital splitting parameter Δ for Mg^{2+} (circles) and Zn^{2+} (open squares) solutions. The thin horizontal lines are time averages.

According to the model proposed in section III, the $1\pi_y/1\pi_x$ energy splitting in $Mg^{2+}(H_2O)_6$ is predominantly of electrostatic origin. Assuming that a similar electrostatic component contributes by the same amount to the splitting in the Zn^{2+} complex, one can then estimate the magnitude of the additional π_x gas-phase stabilization arising exclusively from orbital interaction in the latter system, $\Delta_{oi} = \Delta[Zn^{2+}] - \Delta[Mg^{2+}] = 0.543 - 0.180 = 0.363$ eV. The corresponding averaged value in solution is $\langle\Delta_{oi}\rangle = \langle\Delta[Zn^{2+}]\rangle - \langle\Delta[Mg^{2+}]\rangle = 0.483 - 0.249 = 0.234$ eV. The decrease in Δ_{oi} in going from isolated to solvated systems is thus sufficiently large to overcome the indeterminacy in orbital energies caused by finite-temperature relaxation and solvent fluctuations.

C. Orbital Interactions in Solvated Zn^{2+}. The lower value of Δ_{oi} points to the existence of an electronic mechanism hindering the $1\pi_x \rightarrow$ 4s charge transfer, which decreases the gain in stability of dissociated $Zn^{2+}(H_2O)_5(OH^-)$ in solution compared to the gas-phase system. This would in turn affect the relative concentrations of $Zn^{2+}(H_2O)_6$ and $Zn^{2+}(H_2O)_5(OH^-)$ at equilibrium, resulting in a *reduced* acidity of hydrated versus gas-phase Zn^{2+}-coordinated water. We will now attempt to provide a qualitative analysis of the origin of this acidity-damping effect.

We consider again the dissociated pseudo-octahedral gas-phase complex $Zn^{2+}(H_2O)_5(OH^-)$. The 4s orbital of Zn contributes non-negligibly to the lowest virtual state of this system (5.10%). As a consequence of the $1\pi_x$−4s orbital mixing, the HOMO-1 (the member of the $1\pi_y/1\pi_x$ pair stabilized by orbital interaction) also carries a substantial Zn 4s character (4.74%). The largest Zn 4s contributions are observed among virtual states at higher energies (e.g., LUMO+6, ∼2.9 eV above the LUMO, with 48.98% Zn 4s character). The splitting parameter for this system is $\Delta = 0.346$ eV.

Changes in the electronic structure of $Zn^{2+}(H_2O)_5(OH^-)$ on solvation were then examined using the COSMO reaction-field approach. The geometry was *not* re-optimized in the presence of the dielectric continuum. As expected, embedding affects the value of Δ which drops to 0.265 eV. The Zn 4s contribution to HOMO-1 decreases to 3.64%, indicating a weakening of the $1\pi_x \rightarrow$ 4s interaction. The LUMO+6, ∼2.7 eV above the LUMO, is now an almost pure (84.91%) Zn 4s state, whereas, rather surprisingly, the 4s contribution to the LUMO is reduced to ∼1%.

To study in detail the effect of structure fluctuations at finite temperature, we then considered a series of fictitious ionic

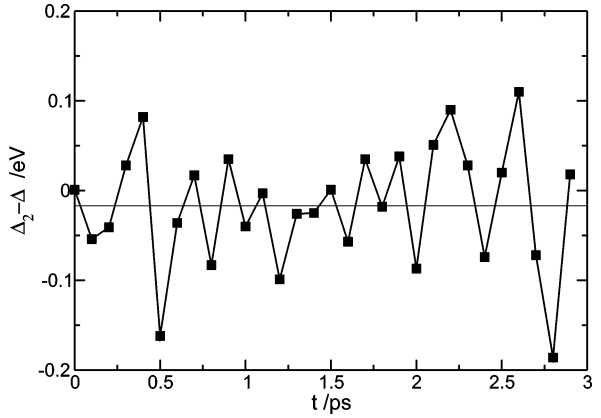

Figure 10. Difference between the splitting parameter for $Zn^{2+}(H_2O)_5(OH^-)(H_3O^+)$ computed using a continuum model (Δ_2) and with an explicit solvent (Δ). The thin horizontal line is the average over time. See text for details.

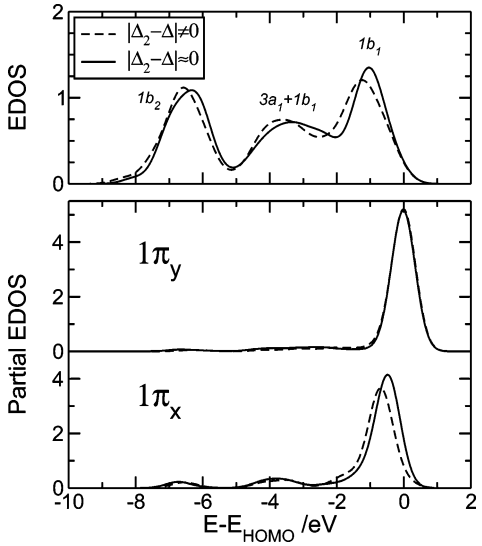

Figure 11. (upper panel) Hydrated Zn^{2+} EDOS for one atomic configuration with large ($|\Delta_2 - \Delta| \neq 0$) and another one with small mismatch between the COSMO estimate and the explicit-solvent orbital splitting parameter. (lower panel) Partial EDOS of π_y and π_x states corresponding to the same two atomic configurations. Energies are all referred to the HOMO. See main text for details.

configurations obtained from AIMD on solvated Zn^{2+} in the dissociated limit. We then eliminated all solvent water molecules from the sample, and we computed the splitting parameter for the resulting ion pair $Zn^{2+}(H_2O)_5(OH^-)(H_3O^+)$ as an isolated gas-phase system without (Δ_1) and with (Δ_2) COSMO embedding. We performed these calculations starting from the same set of instantaneous atomic configurations used for the estimate of $\langle\Delta\rangle$ in solution (see above). The corresponding averages over 3 ps were $\langle\Delta_1\rangle = 0.675$ eV and $\langle\Delta_2\rangle = 0.500$ eV (Figure 10). The splitting parameter decreases on average by ~26% upon embedding, a value which is very close to the relative reduction in the pseudo-octahedral complex (~23%). Besides, the destabilization of the 4s orbital upon inclusion into the dielectric is rather insensitive to the overall charge of the complex, +1 in the pseudo-octahedral system and +2 in the ion pair. Overall, this analysis shows that the long-range, electrostatic perturbation of the dielectric medium acts by selectively shifting Zn 4s character from the lowest region of the conduction band of the solution toward higher energies. The charge-transfer $1\pi_x$ state is destabilized because of reduced OH^- $1\pi_x$−Zn 4s orbital interaction caused by less favorable energy matching compared to hypothetical gas-phase $Zn^{2+}(H_2O)_5(OH^-)(H_3O^+)$.

Finally, we note that the COSMO estimate $\langle\Delta_2\rangle$ is in good agreement with the splitting parameter computed from the Zn^{2+} AIMD simulation with an explicit solvent, $\langle\Delta\rangle = 0.483$ eV. This suggests that, *on average*, an implicit solvation model may yield a sufficiently faithful representation of the perturbed electronic structure of the solvated system. The average response of the solvent is therefore, as expected, well represented by the continuum approach. Nonetheless, we regard an explanation of the drop in acidity of Zn^{2+}-coordinated water in solution based exclusively on electrostatic arguments as incomplete. The highly flexible nature of the first solvation shell of Zn^{2+} enhances the sensitivity of Δ to thermal fluctuations in the microscopic structure of the solvent. This brings about wide variations of this quantity over time: deviations from the average value (0.483 eV) may be as large as ~0.25 eV. In some configurations, the mismatch between the COSMO estimate Δ_2 and the actual Δ in solution may reach 0.2 eV, and only when averaged over time do the two quantities agree to within ~0.02 eV. In Figure 11, we show EDOS plots of one AIMD atomic configuration for which the COSMO estimate of the splitting parameter differs substantially from the explicit-solvent value ($|\Delta_2 - \Delta| \neq 0$) and of one for which the two models are closely in agreement ($|\Delta_2 - \Delta| \simeq 0$). In the lower panel, we show partial EDOS profiles for the $1\pi_y$ and the charge-transfer $1\pi_x$ states. The former corresponds to the HOMO in both atomic configurations. Electronic bands of the solution are conventionally labeled here according to the symmetry of molecular orbitals of a water molecule in the gas phase.[71] The $1\pi_x$ state is responsible for a main peak in the valence $1b_1$ band of the solution and for minor contributions to the $3a_1 + 1b_1$ and $1b_2$ bands. Its larger spread in energy compared to $1\pi_y$ indicates a more pronounced tendency to hybridize with solvent water molecules. The main peak of the "anomalous" $|\Delta_2 - \Delta| \neq 0$ configuration shows a a tendency to spread toward lower energies and, possibly, to develop a second minor shoulder some 1 eV below the main feature. We interpret this as an enhancement in the orbital mixing with solvent states belonging to the valence band of the solution. Overall, $1\pi_x$-solvent hybridization reduces the ability of $1\pi_x$ to act as a donor species in the electron transfer to the rather localized Zn 4s state. This mechanism acts as an additional factor in destabilizing the $\pi_x \rightarrow$ 4s charge-transfer state. Such an effect is evidently not accounted for by a solvation model in which only water molecules belonging to the first solvation shell of the cation are treated explicitly.

V. Summary and Conclusions

We have studied the dissociation of water molecules coordinated to a metal center $M^{2+} = Mg^{2+}$, Zn^{2+} using DFT and AIMD methods. We computed acid dissociation constants via thermodynamic integration of constrained AIMD simulations carried out at room temperature, and we were able to reproduce essentially at a quantitative level the experimentally observed increase in acidity of Zn^{2+}-coordinated, as compared to Mg^{2+}-coordinated, water molecules. A larger error (~1 p*K* unit) was observed in absolute (i.e., relative to clean water) acidities.

On the basis of analysis of the electronic structure of the microsolvated metal ions in the gas phase, we showed that the lower pK_a of Zn^{2+}-coordinated versus Mg^{2+}-coordinated water molecules is largely a manifestation of a specific orbital interaction between a π state of the OH^- group and the 4s orbital of the cation. This covalent component was shown to contribute to the Zn^{2+}−OH^- interaction both in gas-phase $Zn^{2+}(H_2O)_5(OH^-)$ clusters and in the solvated system but to be substantially

reduced in solution. Two mechanisms were found to be responsible for this reduction: destabilization of the 4s state of the cation due to long-range Coulomb interaction with the solvent medium and (to a lesser extent) delocalization of the OH^- state involved in the orbital mixing by hybridization with valence-band states of the solution. We emphasize that the role of the solvent is in this case not limited to (differential) solvation energies for the various species in vacuo. Long-range dielectric effects influence significantly the one-electron states of the metal complexes and, hence, the energetics of the overall orbital interaction.

Acknowledgment. This work was supported by the Dutch National Research School Combination "Catalysis by Design" (NRSC-C). Computer resources were provided by the Netherlands' Scientific Research Council (NWO) through a grant from Stichting Nationale Computerfaciliteiten (NCF).

References and Notes

(1) Tainer, J. A.; Roberts, V. A.; Getzoff, E. D. *Curr. Opin. Biotechnol.* **1991**, *2*, 582.
(2) Douglas, B.; McDaniel, D.; Alexander, J. In *Concepts and Models of Inorganic Chemistry*; John Wiley & Sons: New York, 1994.
(3) Bock, C. W.; Katz, A. K.; Glusker, J. P. *J. Am. Chem. Soc.* **1995**, *117*, 3754.
(4) Caminiti, R.; Licheri, G.; Piccaluga, G.; Pinna, G. *Chem. Phys. Lett.* **1977**, *47*, 275.
(5) Matwiyoff, N. A.; Taube, H. *J. Am. Chem. Soc.* **1968**, *90*, 2796.
(6) Pye, C. C.; Rudolph, W. W. *J. Phys. Chem. A* **1998**, *102*, 9933.
(7) Wakita, H.; Johansson, G.; Sandström, M.; Goggin, P. L.; Ohtaki, H. *J. Solution Chem.* **1991**, *20*, 643.
(8) Johansson, G. *Adv. Inorg. Chem.* **1992**, *39*, 159.
(9) Ohtaki, H.; Radnai, T. *Chem. Rev.* **1993**, *93*, 1157.
(10) Fatmi, M. Q.; Hofer, T. S.; Randolf, B. R.; Rode, B. M. *J. Chem. Phys.* **2005**, *123*, 054514.
(11) Marini, G. W.; Texler, N. R.; Rode, B. M. *J. Phys. Chem.* **1996**, *100*, 6808.
(12) Pavlov, M.; Siegbahn, P. E. M.; Sandström, M. *J. Phys. Chem. A* **1998**, *102*, 219.
(13) Rudolph, W. W.; Pye, C. C. *Phys. Chem. Chem. Phys.* **1999**, *1*, 4583.
(14) Lee, S.; Kim, J.; Park, J. K.; Kim, K. S. *J. Phys. Chem.* **1996**, *100*, 14329.
(15) Lightstone, F. C.; Schwegler, E.; Hood, R. Q.; Gygi, F.; Galli, G. *Chem. Phys. Lett.* **2001**, *343*, 549.
(16) Blumberger, J.; Bernasconi, L.; Tavernelli, I.; Vuilleumier, R.; Sprik, M. *J. Am. Chem. Soc.* **2004**, *126*, 3928.
(17) Pasquarello, A.; Petri, I.; Salmon, P. S.; Parisel, O.; Car, R.; Thot, E.; Powell, D. H.; Fischer, H. E.; Helm, L.; Merbach, A. E. *Science* **2001**, *291*, 856.
(18) Bakó, I.; Hutter, J.; Pálinkás, G. *J. Chem. Phys.* **2002**, *117*, 9838.
(19) Marx, D.; Sprik, M.; Parrinello, M. *Chem. Phys. Lett.* **1997**, *273*, 360.
(20) Ensing, B.; Buda, F.; Baerends, E. J. *J. Phys. Chem. A* **2003**, *107*, 5722.
(21) Ensing, B.; Buda, F.; Gribnau, M. C.; Baerends, E. J. *J. Am. Chem. Soc.* **2004**, *126*, 4355.
(22) Bickmore, B. R.; Tadanier, C. J.; Rosso, K. M.; Monn, W. D.; Egget, D. L. *Geochim. Cosmochim. Acta* **2004**, *68*, 2025.
(23) Klamt, A.; Eckert, F.; Diedenhofen, M.; Beck, M. E. *J. Phys. Chem. A* **2003**, *107*, 9380.
(24) Eckert, F.; Klamt, A. *J. Comput. Chem.* **2006**, *27*, 11.
(25) Chipman, D. M. *J. Phys. Chem. A* **2002**, *106*, 7413.
(26) Kelly, C. P.; Cramer, C. J.; Truhlar, D. G. *J. Phys. Chem. A* **2006**, *110*, 2493.
(27) Saracino, G. A. A.; Improta, R.; Barone, V. *Chem. Phys. Lett.* **2003**, *373*, 411.
(28) Topol, I. A.; Tawa, G. J.; Caldwell, R. A.; Eissenstat, M. A.; Burt, S. K. *J. Phys. Chem. A* **2000**, *104*, 9619.
(29) Liptak, M. D.; Shields, G. C. *J. Am. Chem. Soc.* **2001**, *123*, 7314.
(30) Almerindo, G. I.; Tondo, D. W.; Pliego, J. R. *J. Phys. Chem. A* **2004**, *108*, 166.
(31) Yang, B.; Wright, J.; Eldefrawi, M. E.; Pou, S.; MacKerell, A. D. J. *J. Am. Chem. Soc.* **1994**, *116*, 8722.
(32) Schüürmann, G.; Cossi, M.; Barone, V.; Tomasi, J. *J. Phys. Chem. A* **1998**, *102*, 6706.
(33) Shapley, R. A.; Bacskay, G. B.; Warr, G. G. *J. Phys. Chem. B* **1998**, *102*, 1938.
(34) Lyne, P. D.; Karplus, M. *J. Am. Chem. Soc.* **2000**, *122*, 166.
(35) Soriano, E.; Cerdán, S.; Ballesteros, P. *J. Mol. Struct. (THEOCHEM)* **2004**, *684*, 121.
(36) Fischer, B. J. *J. Org. Chem.* **2002**, *67*, 790.
(37) Jorgensen, W. L.; Briggs, J. M.; Gao, J. *J. Am. Chem. Soc.* **1987**, *109*, 6857.
(38) Martínez, J. M.; Pappalardo, R. R.; Marcos, E. S. *J. Phys. Chem. A* **1997**, *101*, 4444.
(39) Martínez, J. M.; Pappalardo, R. R.; Marcos, E. S.; Mennucci, B.; Tomasi, J. *J. Phys. Chem. B* **2002**, *106*, 1118.
(40) Davies, J. E.; Doltsinis, N. L.; Kirby, A. J.; Roussev, C. D.; Sprik, M. *J. Am. Chem. Soc.* **2002**, *124*, 6594.
(41) Ivanov, I.; Klein, M. L. *J. Am. Chem. Soc.* **2002**, *124*, 13380.
(42) Ivanov, I.; Chen, B.; Raugei, S.; Klein, M. L. *J. Phys. Chem. B* **2006**, *110*, 6365.
(43) Chandler, D. In *Introduction to Modern Statistical Mechanics*; Oxford University Press: New York, 1987.
(44) Gilson, M. K.; Given, J. A.; Bush, B. L.; McCammon, J. A. *Biophys. J.* **1997**, *72*, 1047.
(45) Strajbl, M.; Hong, G.; Warshel, A. *J. Phys. Chem. B* **2002**, *106*, 13333.
(46) Becke, A. *Phys. Rev. A* **1988**, *38*, 3098.
(47) Lee, C.; Yang, W.; Parr, R. G. *Phys. Rev. B* **1988**, *37*, 785.
(48) *ADF2005.01*; SCM, Theoretical Chemistry; Vrije Universiteit Amsterdam: The Netherlands, 2005 (http://www.scm.com).
(49) van Lenthe, E.; van Leeuwen, R.; Baerends, E. J.; Snijders, J. G. *Int. J. Quantum Chem.* **1996**, *57*, 281.
(50) Klamt, A.; Schüürmann, G. *J. Chem. Soc., Perkin Trans.* **1993**, *2*, 799.
(51) Pye, C. C.; Ziegler, T. *Theor. Chem. Acc.* **1999**, *101*, 396.
(52) Klamt, A.; Jonas, V.; Bürger, T.; Lohrenz, J. C. W. *J. Phys. Chem.* **1998**, *102*, 5074.
(53) Sillanpää, A. J.; Aksela, R.; Laasonen, K. L. *Phys. Chem. Chem. Phys.* **2003**, *5*, 3382.
(54) *CPMD*, version 3.9.1; Festkörperforschung Stuttgart and IBM Zurich Research Laboratory, 2004 (http://www.cpmd.org).
(55) Kleinman, L.; Bylander, D. M. *Phys. Rev. Lett.* **1982**, *48*, 1425.
(56) Troullier, N.; Martins, J. L. *Phys. Rev. B* **1991**, *43*, 1993.
(57) Louie, S. G.; Froyen, S.; Cohen, M. L. *Phys. Rev. B* **1982**, *26*, 1982.
(58) Qteish, A.; Needs, R. J. *Phys. Rev. B* **1991**, *43*, 4229.
(59) Kuzmin, A.; Obst, S.; Purans, J. *J. Phys.: Condens. Matter* **1997**, *9*, 10065.
(60) Car, R.; Parrinello, M. *Phys. Rev. Lett.* **1985**, *55*, 2471.
(61) Remler, D. K.; Madden, P. A. *Mol. Phys.* **1990**, *70*, 921.
(62) Marx, D.; Hutter, J. In *Modern Methods and Algorithms of Quantum Chemistry*; Grotendorst, J., Ed.; John von Neumann Institute for Computing: Jülich, Germany, 2000; Vol. 1, p 329.
(63) Thermodynamic properties of the gas-phase complexes were estimated from standard thermal analysis of the temperature-dependent partition function, as implemented in ADF. See http://www.scm.com for further details.
(64) Bickelhaupt, F. M.; Baerends, E. J. *Rev. Comput. Chem.* **2000**, *15*, 1.
(65) Marcus, Y. *Chem. Rev.* **1988**, *88*, 1475.
(66) Arab, M.; Bougeard, D.; Smirnov, K. S. *Chem. Phys. Lett.* **2003**, *379*, 268.
(67) Carter, E. A.; Ciccotti, G.; Hynes, J. T.; Kapral, R. *Chem. Phys. Lett.* **1989**, *156*, 472.
(68) Sprik, M.; Ciccotti, G. *J. Chem. Phys.* **1998**, *109*, 7737.
(69) Trout, B. L.; Parrinello, M. *J. Phys. Chem. B* **1999**, *103*, 7340.
(70) Sprik, M. *Chem. Phys.* **2000**, *258*, 139.
(71) do Couto, P. C.; Estácio, S. G.; Cabral, B. J. C. *J. Chem. Phys.* **2005**, *123*, 054510.